

## Formation of Kaonic Atoms and Kaonic Nuclei by In-flight ( $K^-$ , $p$ ) reactions

Junko YAMAGATA, Hideko NAGAIRO, Yuko OKUMURA<sup>\*)</sup> and Satoru HIRENZAKI

*Department of Physics, Nara Women's University, Nara 630-8506, Japan*

(Received )

We study the kaonic atom and kaonic nucleus formation by the in-flight ( $K^-$ ,  $p$ ) reactions for C, O, Si and Ca target cases theoretically. Deeply bound kaonic atoms were predicted to exist as quasi-stable states and were expected to be observed in some proper experimental methods. Kaonic nuclear states are also expected to exist with large decay widths. We evaluate the formation cross sections of the kaonic atoms and kaonic nuclei using an effective number approach. We show that the indications of the kaonic bound states can be observed in the outgoing proton energy spectra.

### §1. Introduction

Kaonic atoms and kaonic nuclei carry important information on the  $K^-$ -nucleon interaction in the nuclear medium. This information is very important for the constraints of kaon condensation in high density matter. The properties of kaons in nuclei are largely influenced by the change of  $\Lambda(1405)$  in the nuclear medium, since  $\Lambda(1405)$  is a resonance state just below the kaon-nucleon threshold. In fact, there were studies of kaonic atoms by modifying the properties of  $\Lambda(1405)$  in the nuclear medium.<sup>1), 2), 3)</sup> These works demonstrated the ability of reproducing the kaonic atom properties, which come out to be as good as the phenomenological study of Batty.<sup>4)</sup>

Recently, there have been very important developments in the description of hadron properties in terms of the SU(3) chiral Lagrangian. The unitarization of the chiral Lagrangian provides the  $\Lambda(1405)$  resonance state as a baryon-meson coupled system.<sup>5), 6)</sup> Then, the properties of  $\Lambda(1405)$  in the nuclear medium using the SU(3) chiral unitary model was also investigated by Waas et al.,<sup>7)</sup> Lutz<sup>8)</sup> and Ramos and Oset.<sup>9)</sup> All of them have considered the Pauli effect on the intermediate nucleons. In addition in Ref. 8) the selfenergy of the kaon in the intermediate states is considered and in Ref. 9) the selfenergies of the pions and baryons are also taken into account. These approaches lead to a kaon selfenergy in the nuclear medium which can be tested with kaonic atoms and kaonic nuclei.

In our previous work,<sup>10)</sup> we adopted the scattering amplitude in the nuclear medium calculated by Ramos and Oset<sup>9)</sup> for the studies of kaonic atoms, and showed the ability of reproducing the existing kaonic atom data as good as the optical potential reported by Batty.<sup>4)</sup> We then calculated the deeply bound kaonic atoms for  $^{16}\text{O}$  and  $^{40}\text{Ca}$ , which had narrow widths and were expected to be observed by proper methods.<sup>11), 12)</sup> We also obtained very deep kaonic nuclear states, which

---

<sup>\*)</sup> Present Address: Ritto High School, Ritto, Shiga, Japan

had large decay widths of the order of several tens of MeV. The  $(K^-, \gamma)$  reaction was studied for the formation of the deeply bound kaonic states<sup>10)</sup> which could not be observed by the kaonic X-ray spectroscopy, using the formulation developed in Ref. 13) for the formation of deeply bound pionic atoms with the  $(\pi^-, \gamma)$  reaction.

Another very important development in these years is in the studies of kaonic nuclear states, which are the kaon-nucleus bound systems mainly due to the strong interaction. The experimental studies of the kaonic nuclear states by the in-flight  $(K, N)$  reactions were proposed and performed by Kishimoto and his collaborators.<sup>14), 15)</sup> The experiments by stopped  $(K, N)$  reactions are carried out by Iwasaki, T. Suzuki and their collaborators and reported in Refs. 16), 17). In these experiments, they have found some indications of the existence of the kaonic nuclear states. There are also theoretical studies of the structure and formation of the kaonic nuclear states related to these experimental activities.<sup>18)</sup> It should be noticed that the theoretical studies predicted the possible existence of the ultra-high density states in the kaonic nuclear systems.<sup>18)</sup>

In this paper, we study the in-flight  $(K^-, p)$  reactions systematically to populate the deeply bound kaonic states and to observe their properties in experiments. We have witnessed the usefulness of the direct reactions for the formation of the deeply bound pionic atoms by using the  $(d, {}^3\text{He})$  reactions.<sup>19), 20), 21), 22)</sup> However, in the present case one would have to produce a  $K^+$  in addition in this  $(d, {}^3\text{He})$  reaction and there would be a large momentum mismatch. For this reason the  $(K^-, \gamma)$  reaction was considered first in Ref. 10). Here we consider another reaction  $(K^-, p)$  theoretically and show the systematic results to know the experimental feasibility of the reaction. The  $(K^-, p)$  reaction was proposed before in Refs. 12), 14), however, the realistic spectra have not been calculated so far. We calculate the expected spectra theoretically using the same approach used in Ref. 20) for the deeply bound pionic atom formation reaction. We think this theoretical evaluation will be interesting and important for the studies of kaon properties in nuclear medium.

In sect. 2, we describe the theoretical model for the structure of the kaon-nucleus bound systems and show the numerical results. Theoretical formalisms and numerical results of the  $(K^-, p)$  reactions are discussed in sect. 3. We give a summary in sect. 4.

## §2. Structure of Kaonic Atoms and Kaonic Nuclei

### 2.1. Formalism

We study the properties of kaonic bound systems by solving the Klein-Gordon equation

$$[-\nabla^2 + \mu^2 + 2\mu V_{\text{opt}}(r)]\phi(\mathbf{r}) = [E - V_{\text{coul}}(r)]^2\phi(\mathbf{r}) . \quad (2.1)$$

Here,  $\mu$  is the kaon-nucleus reduced mass and  $V_{\text{coul}}(r)$  is the Coulomb potential with a finite nuclear size:

$$V_{\text{coul}}(r) = -e^2 \int \frac{\rho_{\text{p}}(r')}{|\mathbf{r} - \mathbf{r}'|} d^3r' , \quad (2.2)$$

where  $\rho_p(r)$  is the proton density distribution. We take the empirical Woods-Saxon form for the density and keep the shapes of neutron and proton density distributions the same:

$$\rho(r) = \rho_n(r) + \rho_p(r) = \frac{\rho_0}{1 + \exp[(r - R)/a]}, \quad (2.3)$$

where we use  $R = 1.18A^{1/3} - 0.48$  [fm] and  $a = 0.5$  [fm] with  $A$  the nuclear mass number.

The kaon-nucleus optical potential  $V_{\text{opt}}$  is written as;

$$2\mu V_{\text{opt}}(r) = -4\pi\eta a_{\text{eff}}(\rho)\rho(r), \quad (2.4)$$

where  $a_{\text{eff}}(\rho)$  is a density dependent effective scattering length and  $\eta = 1 + m_K/M_N$ . In this paper, we apply two kinds of the effective scattering length, which are the results obtained by the chiral unitary approach<sup>9)</sup> and one of the results of a phenomenological fit.<sup>23)</sup> Here, we do not introduce any energy dependences for the effective scattering lengths, and we use the scattering lengths at the KN threshold energy. The  $a_{\text{eff}}$  of the chiral unitary approach is described in Ref. 10) in detail, which is defined by the kaon self-energy in nuclear matter with the local density approximation. The  $a_{\text{eff}}$  of the phenomenological fit is one of the results reported in Ref. 23) and is parameterized as;

$$a_{\text{eff}}(\rho) = (-0.15 + 0.62i) + (1.66 - 0.04i)(\rho/\rho_0)^{0.24}[\text{fm}]. \quad (2.5)$$

The reason why we consider these two potentials is that the both potentials provide equivalently good descriptions to the observed kaonic atom data even they have much different potential depths as we will see in next subsection. Thus, it should be extremely interesting to see the consequences of these potentials in the ( $K^-$ ,  $p$ ) reaction spectra including kaonic nuclear region.

We solve the Klein-Gordon equation numerically following the method of Oset and Salcedo.<sup>24)</sup> The application of the method to the pionic atom studies were reported in detail in Ref. 25).

## 2.2. Numerical results

We show the kaon nucleus potential for the  $^{39}\text{K}$  case in Fig. 1 as an example. Since the real part of  $a_{\text{eff}}(\rho)$  changes its sign at a certain nuclear density in both chiral unitary and phenomenological models, the kaon nucleus optical potential is attractive while keeping the repulsive sign for the kaon-nucleon scattering length in the free space.

The real part of the scattering length of the phenomenological fit depends on the density much more strongly than the results of chiral unitary model and gives  $\text{Re } a_{\text{eff}}(\rho_0) = 1.51$ [fm]. Hence, as we can see in Fig. 1, the depths of the real optical potentials are significantly different each other for these models. On the other hand, the density dependence of the imaginary part of the phenomenological scattering length is rather flat and the strength is similar to that of the chiral unitary model.

The calculated energy levels for atomic states and nuclear states in  $^{39}\text{K}$  are shown in Fig. 2, where the results of the chiral model and those of the phenomenological

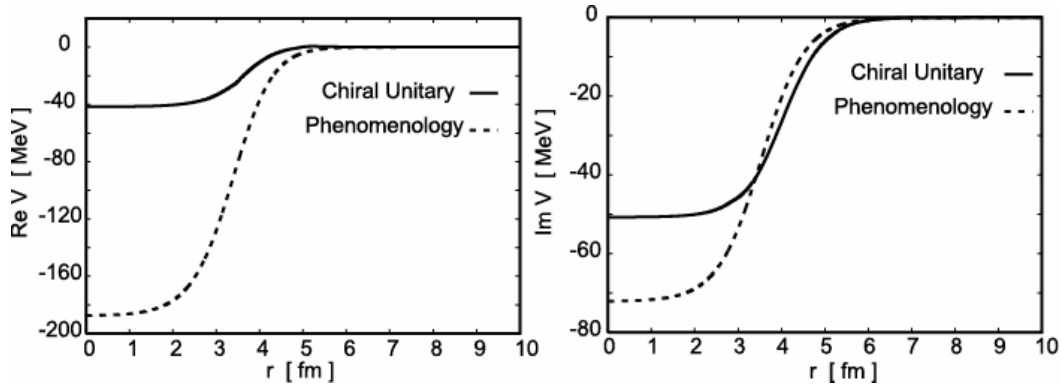


Fig. 1. The kaon-nucleus optical potential for  $^{39}\text{K}$  as a function of the radius coordinate  $r$ . The left and right panels show the real and imaginary part, respectively. The solid line indicates the potential strength of the chiral unitary approach and the dashed line of the phenomenological fit.

model Eq. (2.5) are compared. We can see that the results obtained with both potentials are very similar in atomic states. We find that the deep atomic states such as atomic 1s in  $^{39}\text{K}$ , still unobserved, appear with narrower widths than the separation between levels and are predicted to be quasistable states. Similar results were reported in previous references.<sup>10), 11)</sup> Since the several model potentials predict the existence of the quasistable deep atomic states, it should be interesting to confirm the states experimentally. On the other hand, the predicted binding energies and widths are so stable and almost independent to the potential models considered here. Hence, it is very difficult to distinguish the theoretical potentials only from the observation of atomic levels.

In lower panels of Fig. 2, we also show the energy levels of the deep nuclear kaonic states of  $^{39}\text{K}$  using the chiral unitary model potential and the phenomenological model potential. The deep nuclear states are shown by solid bars with the numbers, which indicate their widths in unit of MeV. These nuclear states have extremely large widths in all cases and will not be observed as peak structures in experiments if they really have such huge widths. We should, however, mention here that the level structures of both potential models are significantly different each other. In chiral unitary potential, only two nuclear states are expected, while the eight states are predicted to exist in phenomenological model. Hence, we may have chance to distinguish the theoretical potentials in observations of kaonic nuclear states.

Calculated density distributions of nuclear 1s and 2s, and atomic 1s kaonic states in  $^{39}\text{K}$  are shown in Fig. 3 for the case with the phenomenological optical potential. The wavefunctions of the deep nuclear kaonic states stay almost inside of the nuclear radius, which is about 3.5 fm for  $^{39}\text{K}$ . Hence, the widths become extremely large of the order of 100 MeV. The wavefunctions of the atomic states are pushed outwards by the imaginary part of the strong interaction. It should be noticed that the atomic 1s state corresponds to the 4-th s state actually in the solutions of the Klein-Gordon (KG) equation Eq. (2.1). We divided the series of KG solutions into two categories which are atomic states and nuclear states since the properties of these states are

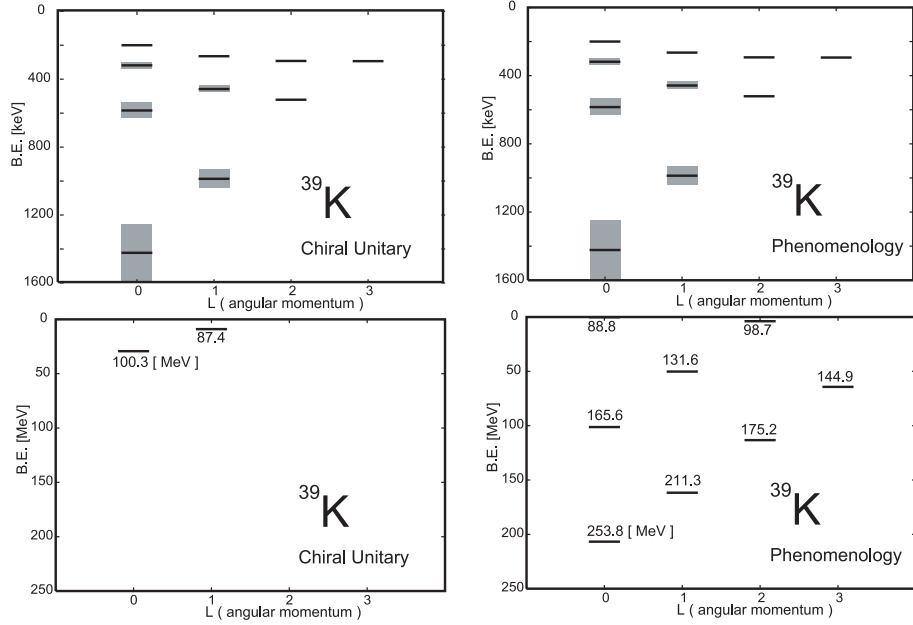


Fig. 2. (Upper panel) Energy levels of kaonic atoms of  $^{39}\text{K}$  obtained with the optical potentials of the chiral unitary model (left) and of the phenomenological fit (right). The hatched area indicates the level widths. (Lower panel) Energy levels of kaonic nuclear states of  $^{39}\text{K}$  obtained with the optical potentials of the chiral unitary model (left) and of the phenomenological fit (right). The level width is indicated by the number at each level in unit of MeV.

much different each other and there are no ambiguities in this classification as you can see in Figs 2, 3.

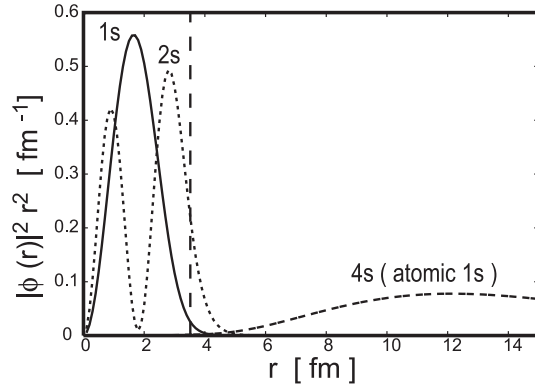


Fig. 3. The kaonic bound state density distributions  $|r\phi(r)|^2$  in coordinate space in  $^{39}\text{K}$  obtained with the phenomenological optical potential. The solid and dotted lines indicate the distribution of the 1s and 2s states. The dashed line is the density of 4s state and is regarded as kaonic atom 1s state. The half-density radius of  $^{39}\text{K}$  is also shown.

We also have calculated the kaon-nucleus binding energies and widths for both atomic and nuclear states in other nuclei. The obtained results are compiled in Table I and Table II for the phenomenological optical potential and for the chiral

unitary potential cases, respectively. We selected  $^{11}\text{B}$ ,  $^{15}\text{N}$ ,  $^{27}\text{Al}$  and  $^{39}\text{K}$  nuclei, which will appear in the final states of the formation reactions for  $^{12}\text{C}$ ,  $^{16}\text{O}$ ,  $^{28}\text{Si}$  and  $^{40}\text{Ca}$  target cases as described in next section. In all cases, we found kaonic atom states and kaonic nuclear states. The results of atomic states resemble each other for both potential cases and are known to reproduce existing data reasonably well. On the other hand, the certain differences are found in kaonic nuclear states energy spectra as expected and they should be investigated experimentally by proper methods.

Table I. Calculated binding energies and widths of kaon- $^{11}\text{B}$ ,  $^{15}\text{N}$ ,  $^{27}\text{Al}$  and  $^{39}\text{K}$  systems with the phenomenological optical potential in unit of MeV for kaonic nuclear states and in unit of keV for kaonic atom states.

Nuclear State (MeV)	$^{11}\text{B}$		$^{15}\text{N}$		$^{27}\text{Al}$		$^{39}\text{K}$	
	B.E.	$\Gamma$	B.E.	$\Gamma$	B.E.	$\Gamma$	B.E.	$\Gamma$
1s	132.5	183.0	155.7	205.5	190.8	239.5	206.7	253.8
2s	-	-	19.0	96.2	69.8	142.3	101.3	165.6
3s	-	-	-	-	-	-	$2.1 \times 10^{-1}$	88.8
2p	58.4	127.0	86.9	151.1	136.3	191.2	161.7	211.3
3p	-	-	-	-	16.5	103.3	50.2	131.6
3d	-	-	22.9	108.3	80.4	152.2	113.3	175.2
4d	-	-	-	-	-	-	3.9	98.7
4f	-	-	-	-	26.2	119.5	64.3	144.9
Atomic State (keV)								
1s	192.4	40.6	338.1	68.2	844.9	243.1	1408.0	355.4
2s	60.5	7.3	111.8	13.3	319.0	58.3	580.6	97.6
3s	29.2	2.5	55.1	4.6	166.8	22.3	316.9	39.9
4s	17.1	1.1	21.7	1.1	102.3	10.8	199.4	20.0
2p	78.5	$6.2 \times 10^{-1}$	154.6	4.0	507.5	37.4	988.7	132.7
3p	34.9	$2.2 \times 10^{-1}$	68.8	1.4	229.4	12.7	458.4	45.8
4p	19.6	$9.6 \times 10^{-2}$	38.7	$6.1 \times 10^{-1}$	130.5	5.7	265.1	20.8
3d	34.9	$2.3 \times 10^{-4}$	69.3	$2.9 \times 10^{-3}$	243.0	$4.2 \times 10^{-1}$	520.9	5.0
4d	19.6	$1.4 \times 10^{-4}$	39.0	$1.7 \times 10^{-3}$	136.6	$2.5 \times 10^{-1}$	292.6	2.9
4f	19.6	$1.0 \times 10^{-8}$	38.9	$4.8 \times 10^{-7}$	136.5	$3.2 \times 10^{-4}$	293.7	$1.7 \times 10^{-2}$

We should mention here that the kaonic nuclear 2p state in  $^{27}\text{Al}$  in Table II provides the negative value for the binding energy. This state is, however, interpreted as to be bound since the corresponding eigen energy in non-relativistic Schrödinger equation has opposite sign to the Klein-Gordon solution due to the large widths of the nuclear states as shown below. The binding energies  $B_{\text{KG}}$  and widths  $\Gamma_{\text{KG}}$  of the Klein-Gordon equation, which are tabulated in Table I and II, are defined as  $E = (\mu - B_{\text{KG}}) - \frac{i}{2}\Gamma_{\text{KG}}$  by the eigen energy  $E$  in Eq. (2.1). The non-relativistic binding energy  $B_{\text{S}}$  and width  $\Gamma_{\text{S}}$  of the Schrödinger equation are related to  $B_{\text{KG}}$  and  $\Gamma_{\text{KG}}$  as;

$$B_{\text{S}} = B_{\text{KG}} - \frac{B_{\text{KG}}^2}{2\mu} + \frac{\Gamma_{\text{KG}}^2}{8\mu}, \quad (2.6)$$

Table II. Calculated binding energies and widths of kaon- $^{11}\text{B}$ ,  $^{-15}\text{N}$ ,  $^{-27}\text{Al}$  and  $^{-39}\text{K}$  systems with the optical potential of chiral unitary model in unit of MeV for kaonic nuclear states and in unit of keV for kaonic atom states.

Nuclear State (MeV)	$^{11}\text{B}$		$^{15}\text{N}$		$^{27}\text{Al}$		$^{39}\text{K}$	
	B.E.	$\Gamma$	B.E.	$\Gamma$	B.E.	$\Gamma$	B.E.	$\Gamma$
1s	4.6	81.6	11.0	87.9	22.5	96.6	29.3	100.3
2p	-	-	-	-	-1.1	79.5	89.7	87.4
Atomic State (keV)								
1s	167.5	35.0	340.5	67.8	852.1	199.1	1422.7	337.3
2s	61.3	6.2	112.3	13.2	320.4	47.6	584.3	92.5
3s	29.5	2.1	55.3	1.6	167.2	18.2	318.3	37.8
4s	17.3	$9.3 \times 10^{-1}$	21.7	1.1	102.5	8.8	200.1	19.0
2p	78.4	$6.3 \times 10^{-1}$	154.4	3.1	507.3	34.8	986.8	109.3
3p	34.8	$2.2 \times 10^{-1}$	68.7	1.1	229.3	11.8	457.7	37.7
4p	19.6	$9.7 \times 10^{-2}$	38.7	$4.8 \times 10^{-1}$	130.5	5.3	264.8	17.1
3d	34.9	$1.6 \times 10^{-4}$	69.3	$2.6 \times 10^{-3}$	243.0	$3.4 \times 10^{-1}$	520.8	4.5
4d	19.6	$9.5 \times 10^{-5}$	39.0	$1.6 \times 10^{-3}$	136.6	$2.0 \times 10^{-1}$	292.6	2.6
4f	19.6	$1.0 \times 10^{-8}$	38.9	$3.7 \times 10^{-7}$	136.5	$2.8 \times 10^{-4}$	293.7	$1.5 \times 10^{-2}$

$$\Gamma_S = \Gamma_{\text{KG}} - \frac{B_{\text{KG}}}{\mu} \Gamma_{\text{KG}}. \quad (2.7)$$

Thus, in the case of the kaonic 2p nuclear state in  $^{27}\text{Al}$  in Table II, the non-relativistic binding energies and widths are  $B_S \sim 0.5\text{MeV}$  and  $\Gamma_S \sim \Gamma_{\text{KG}}$ , which indicate that the state is bound.

### §3. Kaonic atoms and Kaonic nuclei formation in ( $K^-$ , $p$ ) reactions

#### 3.1. Formalism

We adopt the theoretical model in Ref. 20) to calculate the formation cross sections of the kaonic atoms and kaonic nuclei in the ( $K^-$ ,  $p$ ) reaction. In the model the emitted proton energy spectra can be written as;

$$\frac{d^2\sigma}{dE_p d\Omega_p} = \left( \frac{d\sigma}{d\Omega} \right)_{K^-p \rightarrow pK^-}^{\text{lab}} \sum_f \frac{\Gamma_K}{2\pi} \frac{1}{\Delta E^2 + \Gamma_K^2/4} N_{\text{eff}}, \quad (3.1)$$

where all (kaon-particle)  $\otimes$  (proton-hole) configurations are summed up in the final kaonic bound states. The differential cross section of the elementary process of the reaction  $K^- + p \rightarrow p + K^-$  in laboratory frame  $(d\sigma/d\Omega)_{K^-p \rightarrow pK^-}^{\text{lab}}$  is evaluated using the  $K^-p$  total elastic cross section data in Ref. 26) by assuming the flat angular distribution in the center of mass frame at each energy. The resonance peak energy is determined by  $\Delta E$  included in Eq. (3.1), which is defined as;

$$\Delta E = T_p - (T_K - S_p(j_p^{-1}) + B_K), \quad (3.2)$$

where  $T_K$  is the incident kaon kinetic energy,  $T_p$  the emitted proton kinetic energy, and  $B_K$  the kaon binding energy in the final state. The proton separation energy  $S_p$  from each single particle level listed in Table III is obtained from data in Refs. 27), 28), 29), 30), 31), 32). We use data in Ref. 33) for the separation energies of the proton-hole levels corresponding to the ground states of daughter nuclei. The widths of the hole states  $\Gamma_p$  are also listed in Table III, which are obtained for the same data sets by assuming the widths of the ground states of daughter nuclei to be zero because of their stabilities.

Table III. One proton separation energies  $S_p$  and widths  $\Gamma_p$  of the hole states of  $^{12}\text{C}$ ,  $^{16}\text{O}$ ,  $^{28}\text{Si}$  and  $^{40}\text{Ca}$  deduced from the data in Ref. 27) for  $^{12}\text{C}$ , in Refs. 28), 29) for  $^{16}\text{O}$ , in Refs. 30), 31) for  $^{28}\text{Si}$ , and in Ref. 32) for  $^{40}\text{Ca}$ . The separation energies corresponding to the ground states of the daughter nuclei are taken from Ref. 33). The widths  $\Gamma_p$  indicate FWHM of Lorentz distribution for  $^{16}\text{O}$  and of Gaussian distributions for other nuclei. The widths of the ground states of the daughter nuclei are fixed to be zero because of their stabilities. For 1p states in  $^{28}\text{Si}$  and  $^{40}\text{Ca}$ , two levels,  $1p_{1/2}$  and  $1p_{3/2}$ , have not been observed separately and, thus, the  $S_p$  and  $\Gamma_p$  are set to be the same values for both levels.

single particle states [MeV]	$^{12}\text{C}$		$^{16}\text{O}$		$^{28}\text{Si}$		$^{40}\text{Ca}$	
	$S_p$	$\Gamma_p$	$S_p$	$\Gamma_p$	$S_p$	$\Gamma_p$	$S_p$	$\Gamma_p$
1d <sub>3/2</sub>							8.3	0
2s <sub>1/2</sub>							11.5	7.7
1d <sub>5/2</sub>					11.6	0	16.3	3.7
1p <sub>1/2</sub>			12.1	0	27.5	17.0	33.2	21.6
1p <sub>3/2</sub>	16.0	0	18.4	$3.1 \times 10^{-6}$	27.5	17.0	33.2	21.6
1s <sub>1/2</sub>	33.9	12.1	41.1	19.0	46.5	21.0	56.3	30.6

The effective number  $N_{\text{eff}}$  is defined as;

$$N_{\text{eff}} = \sum_{JMm_s} \left| \int d^3r \chi_f^*(\mathbf{r}) \xi_{1/2, m_s}^* [\phi_{l_K}^*(\mathbf{r}) \otimes \psi_{j_p}(\mathbf{r})]_{JM} \chi_i(\mathbf{r}) \right|^2. \quad (3.3)$$

The proton and the kaon wavefunctions are denoted as  $\psi_{j_p}$  and  $\phi_{l_K}$ . We adopt the harmonic oscillator wavefunction for  $\psi_{j_p}$ . The spin wave function is denoted as  $\xi_{1/2, m_s}$ , and we take the spin average with respect to  $m_s$  so as to take into account the possible spin direction of the protons in the target nucleus.  $\chi_i$  and  $\chi_f$  are the initial and final distorted waves of the projectile and ejectile, respectively. We use the eikonal approximation and replace  $\chi_f$  and  $\chi_i$  as;

$$\chi_f^*(\mathbf{r}) \chi_i(\mathbf{r}) = \exp(i\mathbf{q} \cdot \mathbf{r}) D(z, \mathbf{b}), \quad (3.4)$$

where  $\mathbf{q}$  is the momentum transfer between the projectile and ejectile and the distortion factor  $D(z, \mathbf{b})$  is defined as;

$$D(z, \mathbf{b}) = \exp \left[ -\frac{1}{2} \sigma_{\text{KN}} \int_{-\infty}^z dz' \rho_A(z', \mathbf{b}) - \frac{1}{2} \sigma_{\text{pN}} \int_z^{\infty} dz' \rho_{A-1}(z', \mathbf{b}) \right]. \quad (3.5)$$

Here, the kaon-nucleon and proton-nucleon total cross sections are denoted as  $\sigma_{\text{KN}}$  and  $\sigma_{\text{pN}}$ .  $\rho_A(z, \mathbf{b})$  and  $\rho_{A-1}(z, \mathbf{b})$  are the density distributions of the target and

the daughter nuclei in beam-direction coordinate  $z$  with an impact parameter  $\mathbf{b}$ , respectively.

We calculate the kaonic bound states wavefunctions using the optical potentials obtained by the chiral unitary model<sup>10)</sup> and the phenomenological fit<sup>23)</sup> as described in Sect. 2. In the chiral unitary model, the depth of the attractive potential is only around 40MeV at the center of the nucleus, which is much weaker than the phenomenological potential in Ref. 23). For the case of the phenomenological potential, there exist kaonic nuclear bound states with huge binding energies like 100 ~ 200 MeV. For these bound states, the  $\bar{K}N$  system can not decay into  $\pi\Sigma$  because of the threshold, and hence, the widths of these states are expected to be narrower. On the other hand for chiral unitary potential cases, we do not have the narrow nuclear states such as in Refs. 14), 18), since the decay phase space for  $\bar{K}N$  system to  $\pi\Sigma$  channel is large enough because of smaller binding energies. In order to introduce the enarrowing effects for the widths due to the phase space suppression, we introduce a phase space factor  $f^{\text{MFG}}$  defined in Ref. 34) by Mareš, Friedman, and Gal as;

$$f^{\text{MFG}}(E) = 0.8f_1^{\text{MFG}}(E) + 0.2f_2^{\text{MFG}}(E), \quad (3.6)$$

where  $f_1^{\text{MFG}}$  and  $f_2^{\text{MFG}}$  are the phase space factors for  $\bar{K}N \rightarrow \pi\Sigma$  decay and  $\bar{K}NN \rightarrow \Sigma N$ , respectively. These factors are defined as;

$$f_1^{\text{MFG}}(E) = \frac{M_{01}^3}{M_1^3} \sqrt{\frac{[M_1^2 - (m_\pi + m_\Sigma)^2][M_1^2 - (m_\Sigma - m_\pi)^2]}{[M_{01}^2 - (m_\pi + m_\Sigma)^2][M_{01}^2 - (m_\Sigma - m_\pi)^2}}} \theta(M_1 - m_\pi - m_\Sigma), \quad (3.7)$$

and

$$f_2^{\text{MFG}}(E) = \frac{M_{02}^3}{M_2^3} \sqrt{\frac{[M_2^2 - (m_N + m_\Sigma)^2][M_2^2 - (m_\Sigma - m_N)^2]}{[M_{02}^2 - (m_N + m_\Sigma)^2][M_{02}^2 - (m_\Sigma - m_N)^2}}} \theta(M_2 - m_\Sigma - m_N). \quad (3.8)$$

Here, the branching ratios of mesic decay and non-mesic decay are assumed to be 80 % and 20%. Masses are defined as  $M_{01} = m_{\bar{K}} + m_N$ ,  $M_1 = M_{01} + E$ ,  $M_{02} = m_{\bar{K}} + 2m_N$ ,  $M_2 = M_{02} + E$ , and  $E$  is the kaon energy defined as  $E = T_K - T_p - S_p$  using the same kinematical variables in Eq. (3.2). We multiply the phase space factor  $f^{\text{MFG}}$  to the energy independent kaonic widths  $\Gamma_K$  to introduce the energy dependence due to the phase space suppression as;

$$\Gamma_K \rightarrow \Gamma_K(E) = \Gamma_K \times f^{\text{MFG}}(E). \quad (3.9)$$

### 3.2. Numerical Results

We show the numerical results for the kaon bound state formation spectra in this subsection. First, we consider the momentum transfer of the ( $K^-$ ,  $p$ ) reactions as a function of the incident kaon energy which is important guide to know the suitable incident energies to get large production rate of the bound states. Since we consider both atomic and nuclear kaon states, we assume four different binding energies to calculate the momentum transfer. We consider the forward reactions and the momentum transfer in laboratory frame is shown in Fig. 4. As can be

seen in the figure, the recoilless condition can be satisfied only for atomic states at  $T_K = 10 \sim 20$  MeV. For deeply bound nuclear states, the reaction always needs a certain momentum transfer. On the other hand, the incident energy dependence of the momentum transfer is not strong for kaonic nuclear states as shown in Fig. 4.

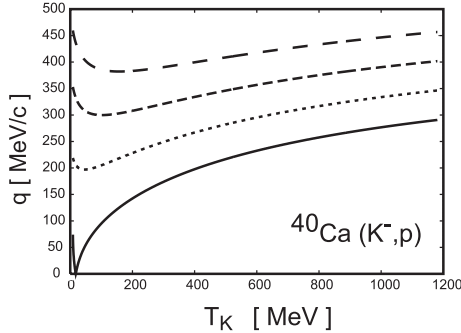


Fig. 4. Momentum transfers in the  $(K^-, p)$  reactions on  $^{40}\text{Ca}$  for the formation of kaon- $^{39}\text{K}$  bound systems. Proton separation energy  $S_p$  is fixed to be 8.3 MeV and kaon binding energies are assumed to be 0 MeV (solid line), 50 MeV (dotted line), 100 MeV (dashed line), and 150 MeV (long-dashed line).

We consider formation of kaonic atoms and kaonic nuclei separately since their properties, and hence, the optimal kinematical conditions for their formation are expected to be different. We consider first the formation of atomic states. Since the binding energies of atomic states are small enough, we can neglect safely the phase space effect for the decay widths considered in Eqs. (3·6)-(3·9). For atomic states, the obtained wavefunctions and energy spectra are almost same for both the chiral unitary and the phenomenological potentials. Hence, we show the results only for chiral unitary potential case.

The energy dependence of the atomic 1s state formation rate is studied in the beginning in order to know the optimal incident energy for the deepest atomic 1s state observation in the  $(K^-, p)$  reactions. For the purpose, we show in Fig. 5 the energy dependence of the ratio of the calculated effective numbers of the kaonic atom 1s and 2p states coupled to  $[d_{3/2}^{-1}]$  proton-hole state in  $^{39}\text{K}$ . We find that the contribution of the 1s state is comfortably larger than that of 2p state at  $T_K=20\text{MeV}$  and we can expect that the 1s state can be observed clearly without large background due to 2p kaonic state at this energy, where the momentum transfer is reasonably small for atomic states formation. Then, we consider the energy dependence of the peak height of the 1s kaonic atom state coupled to  $[d_{3/2}^{-1}]$  proton-hole state in  $^{39}\text{K}$  to know the suitable incident energy to have the large cross section. As we can see in Fig. 6, the cross section takes the highest value around  $T_K=30 - 40$  MeV. And we find that the cross section will have a local maximum value around  $T_K = 400$  MeV. From these observations, we take  $T_K=20$  and 400 MeV as the incident kaon energies where we calculate the energy spectrum of the emitted proton. We also consider  $T_K=100$  MeV as an energy between 20 and 400 MeV. We should mention here that the eikonal approximation is known to be valid only for high energies. Thus, the results for low energies  $T_K \leq 100$  MeV should be considered as rough estimations.

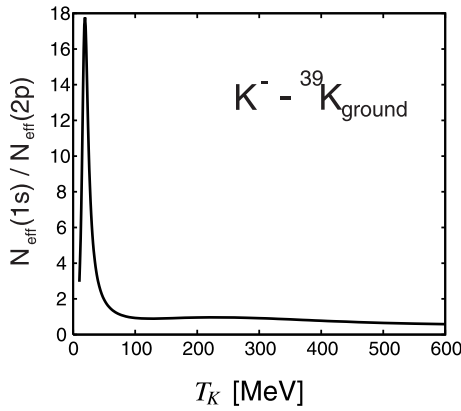


Fig. 5. Ratio of the effective numbers of the 1s and 2p kaonic atom states formation with  $[d_{3/2}^{-1}]$  proton-hole state in  $^{39}\text{K}$  is plotted as a function of the incident kaon energy  $T_K$ .

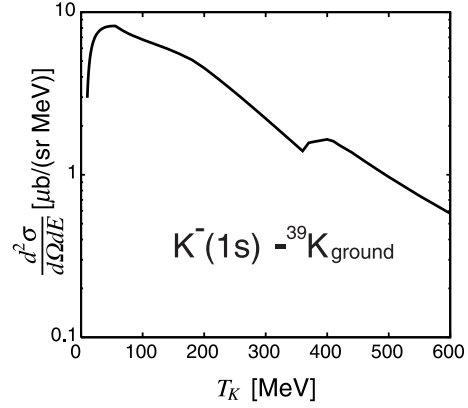


Fig. 6. Double differential cross section at the resonance peak energy of the kaonic atom 1s state formation with  $[d_{3/2}^{-1}]$  proton-hole state in  $^{39}\text{K}$  at  $\theta_p^{\text{Lab}}=0$  [degree] is plotted as a function of the incident kaon kinetic energy.

In Fig. 7 we show the calculated spectra for  $^{40}\text{Ca}$  target including contributions from the kaonic atom states up to 4f for each  $[1d_{3/2}^{-1}]$ ,  $[1d_{5/2}^{-1}]$  and  $[2s_{1/2}^{-1}]$  proton state in  $^{39}\text{K}$  at  $T_K=20$  MeV. The spectra without the widths of the proton-hole states  $\Gamma_p$  are shown by the dashed line. We find that the contributions coupled to different proton-hole states are localized in different energy regions and are well separated from each other. This feature of the spectra is different from that of the pionic atom formation in ( $d, ^3\text{He}$ ) reaction,<sup>20)</sup> where the contributions from different neutron-hole states overlap each other. We also find the same features of the spectra for other incident energies.<sup>35)</sup> The realistic spectra including  $\Gamma_p$  are shown by the solid lines in the same figure. As can be seen in the figure,  $\Gamma_p$  is too large to identify each kaonic bound state except for the  $[d_{3/2}^{-1}]$  hole state corresponding to the ground state of the final daughter nucleus  $^{39}\text{K}$ .

We show in Fig. 8 the detailed structure of the kaonic atom formation cross section coupled to the ground state of the daughter nucleus  $^{39}\text{K}$ . Contributions from deeper proton-hole states will be the smooth background of the spectra in this energy region because of their large widths. We find that the contributions from deeply bound 1s and 2p kaonic atom states are well separated from each other. At  $T_K=20$  MeV, the peak due to 1s state is significantly larger than that of 2p state as expected from the result in Fig. 5. The peak height of the atomic 1s contribution is around 7  $[\mu\text{b}/(\text{sr MeV})]$  at  $T_K=20$  and 100 MeV. At  $T_K=100$  MeV, the 2p peak is enhanced and is around 24  $[\mu\text{b}/(\text{sr MeV})]$ . The whole shapes of the cross section at 100 MeV and 400 MeV resemble each other, while the absolute strength at 400 MeV is around  $1/3 \sim 1/4$  of that of 100MeV.

We then consider the formation spectra of the kaonic nuclear states in the ( $K^-$ ,  $p$ ) reactions. We select the incident kaon energy as to be  $T_K = 600$  MeV, where the experimental data are available.<sup>15)</sup> We show in Fig. 9, the formation spectra of

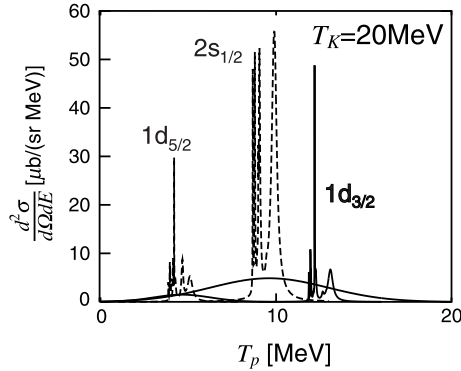


Fig. 7. Kaonic atom formation cross sections for each proton-hole state in the  $(K^-, p)$  reactions are plotted as a function of emitted proton energy at the incident kaon energy  $T_K=20$  MeV and  $\theta_p^{\text{Lab}}=0$  [degree]. The solid and dashed lines are results with and without the widths of the proton-hole states, respectively.

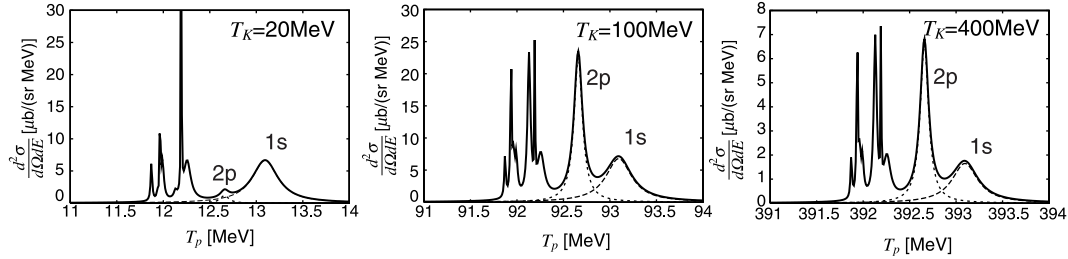


Fig. 8. Kaonic atom formation cross sections in  $^{40}\text{Ca}(K^-, p)$  reactions coupled to  $[d_{3/2}^{-1}]$  proton-hole state in  $^{39}\text{K}$  are plotted as a function of emitted proton energy at  $\theta_p^{\text{Lab}}=0$  [degree] at incident kaon energies  $T_K=20$  MeV, 100 MeV and 400MeV respectively.

kaonic nuclei together with those of kaonic atoms as functions of the emitted proton kinetic energies. Here, the widths of the kaonic states are fixed to be constant as listed in Table I and II. The effects of proton-hole widths  $T_p$  are included. We have found that the spectra does not show any peak-like structure due to the nuclear states formation but only show the smooth slope for both chiral unitary and phenomenological optical potential cases. The contributions from the atomic states formation are found as very narrow two peaks around threshold energies for both potential cases. Each peak contains the several peaks due to the formation of several atomic states like a spectrum shown in Fig. 8.

In order to include the phase space effects on the decay widths for the final kaon system, we multiply the phase space factor defined in Eq. (3.6)-(3.9) to the widths of kaonic states  $T_K$  and calculate the  $(K^-, p)$  spectra. We show the results in Fig. 10 for both potential cases. We find that the spectrum for chiral unitary potential has not been affected much by the phase space effect. However, the  $(K^-, p)$  spectrum shape for the phenomenological potential is distorted by including the phase space factor and is expected to show certain bumpy structure as reported in Ref. 15).

We performed the systematic calculations for other target nuclei,  $^{12}\text{C}$ ,  $^{16}\text{O}$ , and

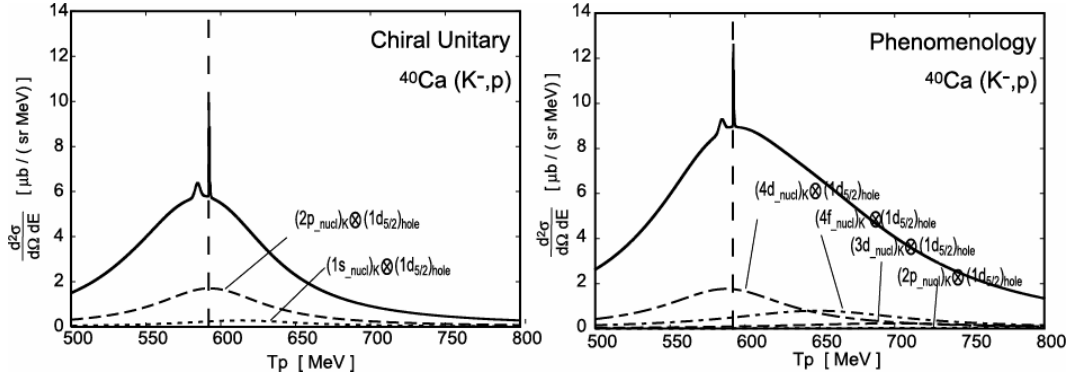


Fig. 9. Kaonic nucleus formation cross sections in  $^{40}\text{Ca}(K^-, p)$  reactions are plotted as functions of emitted proton energies at  $\theta_p^{\text{Lab}} = 0$  [degree] and  $T_K = 600$  MeV for (left) chiral unitary model and (right) phenomenological K-nucleus optical potential cases. The vertical dashed lines indicate the threshold energies and the sharp peaks around the threshold are due to the atomic states formations.

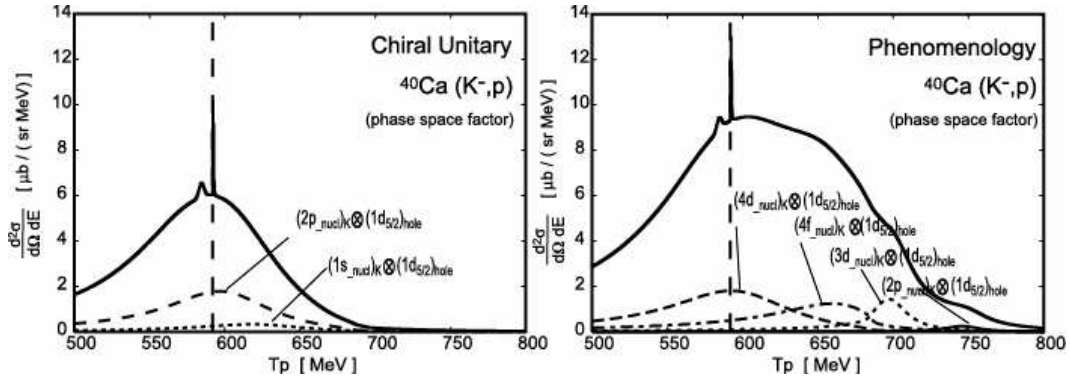


Fig. 10. Kaonic nucleus formation cross sections in  $^{40}\text{Ca}(K^-, p)$  reactions are plotted as functions of emitted proton energies at  $\theta_p^{\text{Lab}} = 0$  [degree] and  $T_K = 600$  MeV for (left) chiral unitary model and (right) phenomenological K-nucleus optical potential cases. The vertical dashed lines indicate the threshold energies and the sharp peaks around the threshold are due to the atomic states formations. The energy dependent decay widths for kaonic states are used. See text in detail.

$^{28}\text{Si}$  at  $T_K = 600$  MeV and show the results in Fig. 11. In Ref. 15), the experimental data with  $^{16}\text{O}$  target is reported and the data with  $^{12}\text{C}$  and  $^{28}\text{Si}$  targets could be obtained in future<sup>36)</sup>. As shown in Fig. 11, we have found that we could expect to find some bumpy structures in the ( $K^-$ ,  $p$ ) spectra due to the formation of the kaon nucleus states, especially in  $^{12}\text{C}$  target case, if the kaon-nucleus optical potential is deep as 200 MeV as reported in Ref. 23). On the other hand, if the depth of the optical potential is shallow as 40 MeV as predicted in chiral unitary model, the spectrum may not show any bumpy structures but only show smooth slope for all targets cases considered here.

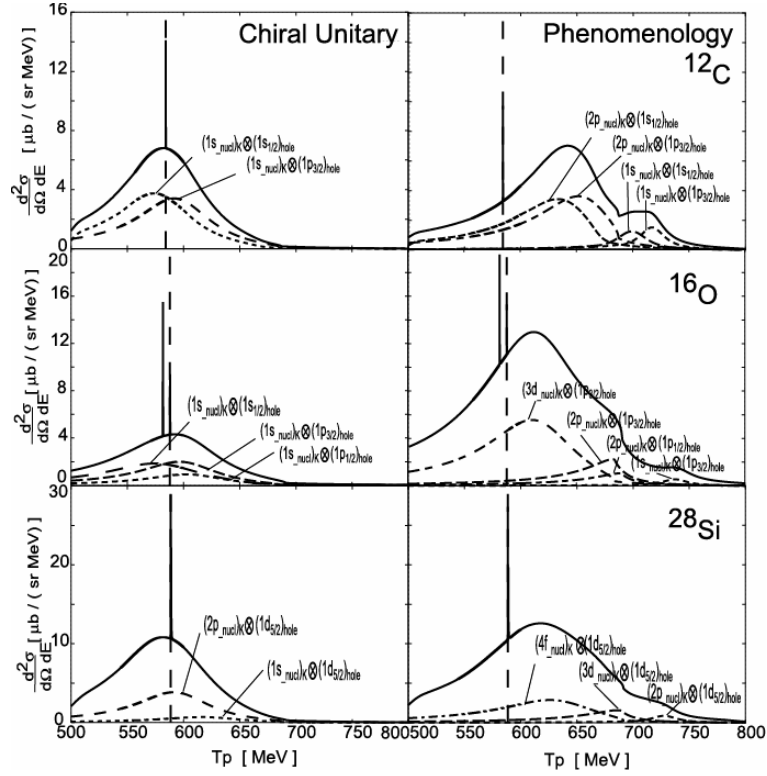


Fig. 11. Same as Fig. 10 except for the target nuclei. Target nuclei are (Top)  $^{12}\text{C}$ , (Middle)  $^{16}\text{O}$ , and (Bottom)  $^{28}\text{Si}$ , respectively.

#### §4. Conclusion

We have studied the structure and formation of kaonic atoms and kaonic nuclei in this paper. We used two different kaon-nucleus optical potentials which are obtained by the chiral unitary model and by the phenomenological fit of existing kaonic atom data. We studied theoretically the structure of kaonic atoms and kaonic nuclei using these potentials and showed the differences of obtained level scheme of kaonic nuclear states.

We also study the formation cross sections of the deeply bound kaonic atoms and kaonic nuclei which can not be observed by the standard X-ray spectroscopy. The all atomic states are predicted to be quasi-stable theoretically. We investigate the  $(K^-, p)$  reaction theoretically and evaluate the cross section of  $^{40}\text{Ca}(K^-, p)$  reaction in detail. For the deep atomic states formation, the cross sections are expected to be around  $7 [\mu\text{b}/(\text{sr MeV})]$  at  $T_K=20$  and  $100$  MeV, and to be around  $2 [\mu\text{b}/(\text{sr MeV})]$  at  $400$  MeV for kaonic atom  $1s$  state formation. For atomic  $2p$  state, the cross section will be around  $24 [\mu\text{b}/(\text{sr MeV})]$  at  $T_K=100$  MeV.

We study the formation cross sections of the kaonic nuclear states in the  $(K^-, p)$  reactions systematically for various target cases, too. In order to take into account the phase space suppression effects of the decay widths, we introduce the phase

space factor to obtain the ( $K^-$ ,  $p$ ) spectra. We found in our theoretical studies that in the ( $K^-$ ,  $p$ ) reactions, the certain bumpy structure due to the kaonic nucleus formation can be seen only for deep ( $\sim 200$  MeV) phenomenological kaon nucleus potential cases. Due to the phase space suppression, the decay widths of kaonic states become so narrow that we can see certain bumpy structure in the reaction spectrum, which could be seen in experiments. As for the chiral unitary potential cases, the binding energies are too small to reduce the decay widths and to see the bumpy structure in the spectra of the ( $K^-$ ,  $p$ ) reactions. However, we should include the energy dependence of the chiral unitary potential properly in the future studies of kaonic nuclear states.

In order to obtain more decisive results theoretically, we need to apply Green function methods for the states with large widths<sup>37)</sup> and to consider energy dependence of the optical potential properly. Furthermore, we should consider the changes and/or deformations of the nucleus due to the existence of kaon inside and solve the problem in self-consistent manner for kaonic nucleus states. However, we believe that the present theoretical efforts to evaluate the absolute cross sections for the kaonic bound states formation are significantly relevant to know the suitable method to observe them, and helpful to develop the physics of kaon-nuclear bound systems and kaon behavior in the nuclear medium. We think we need further investigations both theoretically and experimentally to understand the kaon behavior in nuclear medium more precisely.

### Acknowledgment

We acknowledge E. Oset and A. Ramos for stimulating discussions on kaon bound systems and chiral unitary model. We like to thank the stimulating discussions with M. Iwasaki and T. Kishimoto on the latest experimental data of kaonic nuclei formation. We also like the thank to T. Yamazaki, Y. Akaishi, and A. Dote for useful discussions on theoretical aspects of kaonic nucleus systems. We are grateful to H. Toki and E. Hiyama for many suggestions and discussions of the kaon-nucleus systems.

### References

- [1] M. Alberg, E. M. Henley and L. Wilets, *Ann. of Phys.* **96** (1976), 43.
- [2] R. Brockmann, W. Weise and L. Tauscher, *Nucl. Phys.* **A308** (1978), 365.
- [3] M. Mizoguchi, S. Hirenzaki and H. Toki, *Nucl. Phys.* **A567** (1994), 893.
- [4] C.J. Batty, *Nucl. Phys.* **A372** (1982), 418.
- [5] N. Kaiser, P.B. Siegel and W. Weise, *Nucl. Phys.* **A594** (1995), 325.
- [6] E. Oset and A. Ramos, *Nucl. Phys.* **A635** (1998), 99.
- [7] T. Waas, N. Kaiser and W. Weise, *Phys. Lett.* **B365** (1996), 12; **B379** (1996), 34;  
T. Waas and W. Weise, *Nucl. Phys.* **A625** (1997), 287.
- [8] M. Lutz, *Phys. Lett.* **B426** (1998), 12.
- [9] A. Ramos and E. Oset, *Nucl. Phys.* **A671** (2000), 481.
- [10] S. Hirenzaki, Y. Okumura, H. Toki, E. Oset and A. Ramos, *Phys. Rev.* **C61** (2000), 055205.
- [11] E. Friedman and A. Gal, *Phys. Lett.* **B459** (1999), 43.
- [12] E. Friedman and A. Gal, *Nucl. Phys.* **A658** (1999), 345.
- [13] J. Nieves and E. Oset, *Phys. Lett.* **B282** (1992), 24.

- [14] T. Kishimoto, Phys. Rev. Lett. **83** (1999), 4701.
- [15] T. Kishimoto et al., Prog. Theor. Phys. Suppl. **149** (2003), 264.
- [16] M. Iwasaki et al., nucl-ex/0310018.
- [17] T. Suzuki et al., Phys. Lett. **B597** (2004), 263.
- [18] Y. Akaishi and T. Yamazaki, Phys. Rev. **C65** (2002), 044005.
- [19] H. Toki and T. Yamazaki, Phys. Lett. **B213** (1988), 129.  
H. Toki, S. Hirenzaki, R. S. Hayano and T. Yamazaki, Nucl. Phys. **A501** (1989), 653.
- [20] S. Hirenzaki, H. Toki and T. Yamazaki, Phys. Rev. **C44** (1991), 2472.  
H. Toki, S. Hirenzaki and T. Yamazaki, Nucl. Phys. **A530** (1991), 679.
- [21] H. Gilg et al., Phys. Rev. **C62** (2000), 025201.
- [22] K. Itahashi et al., Phys. Rev. **C62** (2000), 025202.
- [23] C. J. Batty, E. Friedman and A. Gal, Phys. Rep. **287** (1997), 385.
- [24] E. Oset and L. L. Salcedo, J. Comput. Phys. **57** (1985), 361.
- [25] J. Nieves, E. Oset, C. Garcia-Recio, Nucl. Phys. **A554** (1993), 509.
- [26] Review of Particle Physics, Particle Data Group, Phys. Lett. **B592** (2004), 1.
- [27] S. L. Belostotskii et al., Sov. J. Nucl. Phys. **41** (1985), 6.
- [28] M. Yosoi et al., Nucl. Phys. **A738** (2004), 451.
- [29] F. Ajzenberg-selove, Nucl. Phys. **A523** (1991), 1.
- [30] J. Mougey et al., Nucl. Phys. **A262** (1976), 461.
- [31] U. Amaldi et al., Phys. Rev. Lett. **13** (1964), 341.
- [32] K. Nakamura et al., Phys. Rev. Lett. **33** (1974), 853.
- [33] R. B. Firestone et al., Table of Isotopes, 8th edition (1996), John Wiley & Sons, Inc.
- [34] J. Mareš, E. Friedman, A. Gal, nucl-th/0407063.
- [35] Y. Okumura, Masther Thesis, Nara Women's University (2000).
- [36] T. Kishimoto, private communication.
- [37] O. Morimatsu and K. Yazaki, Nucl. Phys. **A435** (1985), 727; **A483** (1988), 493.